ILMENITE DETECTION ON THE MOON BY REMOTE SENSING: AN INTEGRATION OF MULTISENSOR DATASETS OVER MARE AUSTRALE AND MARE INGENII REGIONS. M. Lemelin[1,2], M. Germain[1], C.-E. Morisset[2], V. Hipkin[2] and K. Goïta[1] [1]Département de Géomatique Appliquée, Université de Sherbrooke, 2500 Boulevard de l'Université, Sherbrooke, Qc, Canada, J1K 2R1, Myriam.Lemelin@USherbrooke.ca, [2]Department of Space Science and Technology, Canadian Space Agency, Qc, Canada.

Introduction: Ilmenite ($FeTiO_3$) is the fourth most abundant mineral on the Moon, after pyroxene, plagioclase and olivine [1]. It is a valuable resource because the titanium (TiO_2) and oxygen it contains could be extracted for *in-situ* resource utilization [1]. Finding ilmenite concentrations would facilitate the establishment of a permanent manned base on the Moon.

Several attempts have been made to map ilmenite concentrations on the lunar surface using various approaches [2-4]. Lucey (2004) [2] modeled 85,000 spectra of lunar soils with various mineral abundances, chemistry, grain sizes and maturity using the radiative transfer model of Hapke [5-6]. He then retreived the mineral composition of each pixel in Clementine UVVIS/NIR (415-2000 nm) data by comparing Clementine spectra with the modeled spectra. Ilmenite concentrations were found to be completely determined by the titanium content. Bokun *et al.* (2010) [3] mapped minerals on the lunar surface based on linear unmixing of Clementine UVVIS/NIR spectra and radiative transfer theory of Hapke [6]. The concentrations of ilmenite could not be determined in area of low titanium content. Li and Li (2011) [4] developed an approach based on genetic algorithms and partial least squares regression using Moon Mineralogy Mapper (M3) hyperspectral data (430-3000 nm). The regression used to map ilmenite necessitates the use of more than 30 spectral bands [4], probably because M3 spectral range does not cover the characteristic portion of ilmenite.

Ilmenite has distinctive reflectance properties in the UV/VIS due to two absorption bands, one near 260-270 nm and one near 500 nm, giving the ilmenite a diagnostic feature of globally low reflectance in the UV/VIS, with blue sloped behaviour between ~250-500 nm and red sloped afterwards [7]. This behavior is different from other lunar minerals which are red sloped between the 250-500 nm interval [7].

The goal of this study is to develop a reliable method to map ilmenite concentrations on the lunar surface, at 400 m spatial resolution, taking into consideration the uniqueness of its reflectance in the UV portion of the spectrum reported by [7].

Data and Methods: We use a method based on the radiative transfer model of Hapke [6] with Clementine UVVIS/NIR and Lunar Reconnaissance Orbiter Camera (LROC) Wide Angle Camera (WAC) multispectral datasets. We use Lunar Prospector Gamma-Ray Spectrometer (LP-GRS) and Clementine-derived iron and titanium maps for validation.

The two most recent LROC-WAC color test mosaics are located on the far side of the Moon, one near *Mare Australe* and the other near *Mare Ingenii*. We use these mosaics to take advantage of UV bands (320, 360 nm) of LROC-WAC dataset (also 415, 565, 605, 645, 690 nm). We have also decided to use the bands that are covered by Clementine UVVIS/NIR (415, 750, 900, 950, 1000, 1100, 1250, 1500, 2000 nm) to expand our spectral coverage. We integrate these two datasets by a relative radiometric normalization, which uses their common band at 415 nm, and their nearly common bands at 690 and 750 nm. This allows to adjust the remaining instrument and geometry effects in those multitemporal/multisensor datasets (Fig. 1).

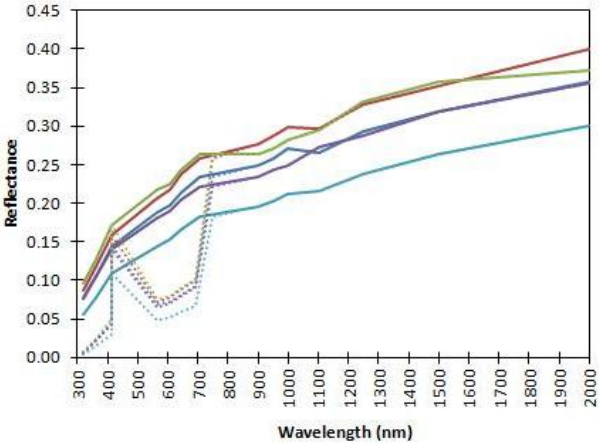

Figure 1. Reflectance spectra of 5 pixels located near *Mare Ingenii* before (dotted lines) and after (solid lines) relative radiometric normalization based on Clementine reflectance at 415 and 750 nm. Before normalization, LRO-WAC reflectance was lower than Clementine reflectance by ~0.8.

We use radiative transfer theory of Hapke [6] to compute reflectance spectra of various mixtures of lunar orthopyroxene, clinopyroxene, plagioclase, olivine and ilmenite, with varying chemistry, grain size nanophase iron abundance. Reflectance spectrum of each pixel is than compared to the modeled spectra, and assigned the composition of the closest match, which minimizes the total difference between the modeled spectra and the pixel spectrum [2]. Ilmenite abundances are compared to existing ilmenite maps [2-3] and to the "maximum possible" ilmenite content map.

To calculate the "maximum possible" ilmenite content, we first determine which iron and titanium algorithms from Clementine data are the most accurate. To evaluate this, we calculate a regression between iron

and titanium maps from LP-GRS [8] and from Clementine UVVIS/NIR algorithms developed over the years [9-16] over ~45,000 pixels in highlands and maria. Optimally, Clementine UVVIS/NIR data can have a spatial resolution of ~100 m, which is more precice than LPGRS data (~15-60 km). The Clementine-derived algorithm of iron and titanium having the highest correlation with its corresponding LP-GRS map is used to derive the maximum possible ilmenite content map. This is done by dividing the abundance of TiO_2 (wt%) in a pixel, by the abundance of TiO_2 (wt%) in stoichiometric ilmenite (52.65). Titanium can also be found in other oxide minerals like ulvöspinel and in volcanis glass [1]. This calculation thus gives the "maximum possible" ilmenite content as it is assuming that all titanium is contained in ilmenite. Stoichiometric ilmenite also contains 47.35 wt% FeO. For our two regions of study, we verify that the iron content of each pixel could account for the maximum concentration of ilmenite calculated.

Initial Results: Analysis of Clementine-derived iron and titanium maps shows that the most suitable algorithms are [11] and [13] respectively, having the highest correlation coefficients (R) and small errors (RSME) (Table 1). These algorithms are computed over our regions of study, generating maps of maximum possible ilmenite content as described above (Fig. 2). *Mare Australe* region has a mean ilmenite content of 1.92 % (1.08 std) up to 6-8 % in some area, whereas *Mare Ingenii* region a mean content of 1.49 % (0.59 std) up to 3-5 %.

Table 1. Regression of iron and titanium mapping algorithms between Clementine-derived algorithms [9-16] and LPGRS maps [8], showing their correlation coefficient (R) and root-mean-square error (RMSE).

FeO	R	RMSE	TiO_2	R	RMSE
[9]	0.92	3.15	[9]	0.70	2.56
[10]	0.85	4.12	[12]	0.73	1.36
[11]	0.94	2.60	[13]	0.74	1.52
[14]	0.91	3.14			
[15]	0.87	3.73			
[16]	0.91	3.29			

Conclusion: The maximum possible ilmenite content for *Mare Australe* and *Mare Ingenii* regions has been calculated using [11,13] algorithms and the composition of stoichiometric ilmenite. These data will be compared to our mineral mapping results. Our innovative mineral mapping method, which integrates LROC-WAC and Clementine UVVIS/NIR datasets, is still ongoing. Through the use of LROC-WAC bandpasses in the UV (320, 360 nm) and between 415-750 nm refining Clementine data, we should be able to map ilmenite with accuracy.

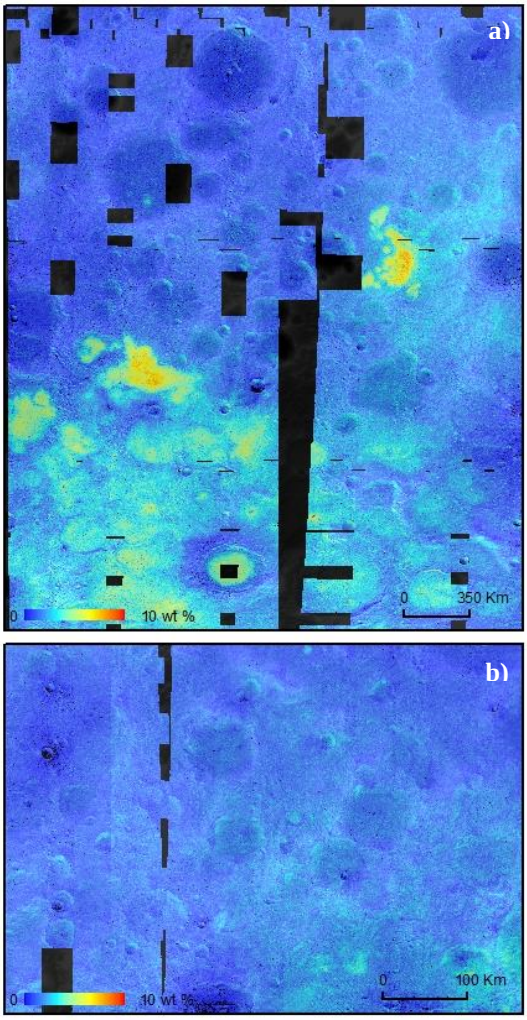

Figure 2. Maximum possible ilmenite content in (a) *Mare Australe* and (b) *Mare Ingenii* regions, on the far side of the Moon, based on iron [11] and titanium [13] algorithms, draped over a Lunar Orbiter Laser Altimeter digital elevation model (black pixels are NoData).

References: [1] Papike, J. et al. (1991) In Heiken, G. H., et al. (Eds.) *Lunar Sourcebook*, Cambridge Univ. Press, New York, pp. 121–181. [2] Lucey, P. G. (2004) *GRL, 31,* L08701. [3] Bokun, Y. et al. (2010) *Icarus, 208,* 11-19. [4] Li, L. and Li, S. (2011) *LPSC XLII*, Abstract #2565. [5] Clark, B. E. (2001) *Meteoritics & Planetary Science, 36*, 1617-1637. [6] Hapke, B. (1993) *Theory of Reflectance and Emittance spectroscopy*, Cambridge Univ. Press, New York, 455p. [7] Cloutis, E. A. et al. (2008) *Icarus, 197,* 321-347. [8] Lawrence, D. J. et al (2011) *Lunar Prospector Reduced Spectrometer Data - Special Products*, http://pds-geosciences.wustl.edu/missions/lunarp/reduced_special.html. [9] Lucey, P. G. et al. (2000) *JGR, 105,* 20,297-20,305. [10] Le Mouélic, S. et al. (2000) *JGR, 105,* 9445-9455. [11] Lawrence, D. J. et al. (2002) *JGR, 107,* E12, 5130. [12] Gillis, J. J. et al. (2003) *JGR, 108,* E2, 5009. [13] Skuratov, Y. G. et al. (2005) *PSS, 53,* 1287-1301. [14] Wilcox, B. B. et al. (2005) *JGR, 110,* E11001. [15] Liu, J. et al. (2007) *CJG, 26,* 98-104. [16] Kramer, G. Y. et al. (2008) *JGR, 113,* E01002.